

Theory of coherent phonons coupled to excitons

Enrico Perfetto^{1,2}, Kai Wu¹ and Gianluca Stefanucci^{1,2}

¹*Dipartimento di Fisica, Università di Roma Tor Vergata, Via della Ricerca Scientifica 1, 00133 Rome, Italy*

²*INFN, Sezione di Roma Tor Vergata, Via della Ricerca Scientifica 1, 00133 Rome, Italy*

* Corresponding Author: Enrico Perfetto

Email address: enrico.perfetto@roma2.infn.it

The interaction of excitons with lattice vibrations underlies the scattering from bright to dark excitons as well as the coherent modulation of the exciton energy. Unlike the former mechanism, which involves phonons with finite momentum, the latter can be exclusively attributed to *coherent phonons* with zero momentum. We here lay down the microscopic theory of coherent phonons interacting with resonantly pumped bright excitons and provide the explicit expression of the corresponding coupling. The coupling notably resembles the exciton-phonon one, but with a crucial distinction: it contains the bare electron-phonon matrix elements rather than the screened ones. Our theory predicts that the exciton energy features a polaronic-like red-shift and monochromatic oscillations or beatings, depending on the number of coupled optical modes. Both the red-shift and the amplitude of the oscillations are proportional to the excitation density and to the square of the exciton-coherent-phonon coupling. We validate our analytical findings through comparisons with numerical simulations of time-resolved optical absorbance in resonantly pumped MoS₂ monolayers.

I. INTRODUCTION

Excitons, bound states formed by one electron and one hole, dominate the photophysics of a wide class of novel functional materials including transition metal dichalcogenides [1–4], perovskites [5–7], Xenes [8–10] and related van der Waals heterostructures [11–13]. The microscopic understanding of the competing processes governing the exciton dynamics is therefore of crucial importance for technological applications in optoelectronics [14–16], photovoltaics [17–19] and photocatalysis [20–22].

The non-equilibrium properties of excitons are largely influenced by the electron-phonon (*e-ph*) coupling g [23], that has been shown to determine excitonic relaxation lifetimes [24–26], optical linewidths [1, 27], energy renormalizations [28], dephasing rates [29–31], and diffusion dynamics [32, 33]. The theoretical description of the exciton dynamics takes advantage from a very useful quantity called exciton-phonon (X-*ph*) coupling [34]. Its expression has been independently derived by a number of authors [34–38] and it involves the projection of the *screened e-ph* coupling $\mathfrak{g} \equiv \varepsilon^{-1}g$ (with ε the dielectric constant) between two excitonic states. Accurate calculations of the X-*ph* coupling have been performed and excellent agreement between theory and experiments has been reported for phonon-assisted photoluminescence spectra [35, 39], exciton linewidths [40, 41], valley depolarization time [42], and polaronic redshifts in absorption spectra [43].

The X-*ph* coupling does not exhaust the possible interactions between excitons and lattice vibrations. Transient optical spectroscopies have recently revealed periodic modulations of the excitonic resonances [44–48], pointing to a strong coupling between excitons and *coherent phonons* (X-*cph*), i.e. waves of atomic vibrations extending over a macroscopic spatial range. In spite of the great interest in the topic, a microscopic theory of the X-*cph* interaction is still lacking.

In this work we show that the X-*cph* coupling G_ν^λ between the lowest bright exciton λ generated after resonant pumping and a coherent phonon mode ν is

$$G_\nu^\lambda = \sum_{\mathbf{k}vc'} g_{cc'}^\nu(\mathbf{k}) A_{\mathbf{k}vc}^{\lambda*} A_{\mathbf{k}vc'}^\lambda - \sum_{\mathbf{k}cvv'} g_{vv'}^\nu(\mathbf{k}) A_{\mathbf{k}v'c}^{\lambda*} A_{\mathbf{k}vc}^\lambda, \quad (1)$$

where $A_{\mathbf{k}vc}^\lambda$ is the exciton wavefunction, $g_{ij}^\nu(\mathbf{k}) = g_{ij}^\nu(\mathbf{k}, \mathbf{q} = 0)$ is the *bare e-ph* coupling for an electron with momentum \mathbf{k} to be scattered from band i to band j by the phonon mode ν (momentum transfer $\mathbf{q} = 0$), and the sum runs over all valence (v) and conduction (c)

bands. We further show that for resonant pumping the X-*cph* coupling is responsible to change the exciton energy in time according to (up to a phase)

$$\delta E^\lambda(\tau) = n \sum_\nu \frac{|G_\nu^\lambda|^2}{\hbar\omega_\nu} \times \left[\frac{n_\nu}{n} \cos \omega_\nu \tau - 1 \right], \quad (2)$$

where $\omega_\nu \equiv \omega_{\nu\mathbf{q}=0}$ is the frequency of the ν -th optical mode at the Γ point, n is the excitation density (number of conduction electrons per unit cell) and $n_\nu \leq n$ are “effective” densities depending on the duration T_P of the pump pulse. The inequality is saturated ($n_\nu = n$) only for T_P shorter than the optical periods $T_\nu = 2\pi/\omega_\nu$ (displacive excitations [49–51]).

The interaction with coherent phonons does not involve a scattering between different excitons, its main effect being a polaronic-like red-shift $-n \sum_\nu \frac{|G_\nu^\lambda|^2}{\hbar\omega_\nu}$ and monochromatic oscillations or beatings (depending on the number of coupled optical modes) of the exciton energy. The polaronic-like red-shift adds up to the one due to (incoherent) phonons [41], which involves the square of the X-*ph* coupling and it is proportional to the number of phonons rather than to the excitation density n . Notably the X-*cph* coupling in Eq. (1) is formally identical to the X-*ph* coupling evaluated at the Γ point for the diagonal scattering $\lambda \rightarrow \lambda$ [34–38], with the crucial difference that the bare g instead of the screened g appears in the former. The difference arises from the diagrammatic origin of these couplings, the X-*cph* one emerging from the Ehrenfest self-energy [52], see below. From Eq. (2) we infer that the amplitude of the coherent oscillations in a time-resolved optical spectrum is proportional to the excitation density and the square modulus of the X-*cph* coupling. This prediction is confirmed through real-time (RT) simulations of transient absorption in resonantly pumped MoS₂ monolayer. Our results provide a readily applicable formula for a quantitative understanding of the coherent dynamics in excitonic materials.

II. RESULTS

Coupling between excitons and coherent phonons

We consider a semiconductor hosting bound excitons, and denote by λ the lowest optically bright exciton. The exciton state is described by the coherent superposition of electron-hole pairs

$$|\lambda\rangle = \sum_{\mathbf{k}vc} A_{\mathbf{k}vc}^\lambda \hat{d}_{\mathbf{k}c}^\dagger \hat{d}_{\mathbf{k}v} |\Phi_0\rangle, \quad (3)$$

where the operator $\hat{d}_{\mathbf{k}i}^{(\dagger)}$ annihilates (creates) an electron with momentum \mathbf{k} in band $i = \{v, c\}$, and $|\Phi_0\rangle$ denotes the ground-state (filled valence bands and empty conduction bands). The exciton wavefunction $A_{\mathbf{k}vc}^\lambda$ is normalized to unity, $\sum_{\mathbf{k}vc} |A_{\mathbf{k}vc}^\lambda|^2 = 1$, and is obtained by solving the Bethe-Salpeter equation (BSE) $HA^\lambda = E^\lambda A^\lambda$ where

$$H_{\mathbf{k}vc, \mathbf{k}'v'c'} = (\epsilon_{\mathbf{k}c} - \epsilon_{\mathbf{k}v})\delta_{\mathbf{k}\mathbf{k}'}\delta_{cc'}\delta_{vv'} + K_{\mathbf{k}vc, \mathbf{k}'v'c'}. \quad (4)$$

Here $\epsilon_{\mathbf{k}v}$ and $\epsilon_{\mathbf{k}c}$ are valence and conduction band dispersions and K is the BSE kernel in the Hartree plus statically screened exchange (HSEX) approximation.

For weak resonant pumping with the exciton energy E^λ the many-body quantum state at time t is well described by $|\Psi(t)\rangle = |\Phi_0\rangle + \sqrt{N(t)} e^{iE^\lambda t} |\lambda\rangle$, where $N(t)$ is the total number of conduction electrons at time t . The weak pumping assumption implies that the excitation density $n(t) = N(t)/N_k \ll 1$, N_k being the number of \mathbf{k} -points in the first Brillouin zone. The change in the one-particle density matrix to lowest order in n is then given by

$$\delta\rho_{\mathbf{k}cc'}(t) = \langle\Psi(t)|\hat{d}_{\mathbf{k}c'}^\dagger \hat{d}_{\mathbf{k}c}|\Psi(t)\rangle = N(t) \sum_v A_{\mathbf{k}vc'}^{\lambda*} A_{\mathbf{k}vc}^\lambda, \quad (5a)$$

$$\delta\rho_{\mathbf{k}vv'}(t) = -\langle\Psi(t)|\hat{d}_{\mathbf{k}v} \hat{d}_{\mathbf{k}v'}^\dagger|\Psi(t)\rangle = -N(t) \sum_c A_{\mathbf{k}vc}^{\lambda*} A_{\mathbf{k}v'c}^\lambda. \quad (5b)$$

Notice that for times subsequent to the end of the pump, i.e., $t > T_P$, $N(t) = N$ is independent of time [53, 54], and so are the density matrix elements for each \mathbf{k} . This peculiarity arises from pumping resonantly with the lowest excitonic state.

The bare $e\text{-}ph$ coupling governs the dynamics of coherent phonons. Let x_ν be the displacement of the ν -th optical mode. To lowest order in n and for times $t > T_P$ it satisfies the equation of motion (EOM) [55]

$$M\ddot{x}_\nu(t) = -M\omega_\nu^2 x_\nu(t) - \frac{1}{x_{0\nu} N_k} \sum_{\mathbf{k}ij} g_{ij}^\nu(\mathbf{k}) \delta\rho_{\mathbf{k}ji}(t), \quad (6)$$

with M the mass of the unit cell and $x_{0\nu} = \sqrt{\hbar/(M\omega_\nu)}$. For resonant pumping we can solve Eqs. (6) with $\delta\rho$ from Eqs. (5). Indeed the phononic feedback on the electronic density matrix yields a correction of order $\mathcal{O}(n^2 g^2)$ that can be neglected. This allows us to rewrite the EOM as

$$\ddot{x}_\nu(t) = -\omega_\nu^2 x_\nu(t) - n(t) \frac{G_\nu^\lambda}{\hbar} \omega_\nu x_{0\nu}, \quad (7)$$

where the X-*cph* coupling G_ν^λ has been defined in Eq. (1). The appearance of the bare *e-ph* coupling g in G_ν^λ implies that the interaction between excitons and coherent phonons can be substantially larger than the interaction between excitons and phonons [56].

Equation (7) admits an analytic solution for any time-dependent excitation density $n(t)$. Let us discuss some physically relevant limiting cases. For displacive excitations [49–51], i.e., if the duration T_P of the pump pulse is much shorter than the phononic period $T_\nu = 2\pi/\omega_\nu$, then we can set $n(t) = n$ and solve Eq. (7) with initial conditions $x_\nu(T_P) = \dot{x}_\nu(T_P) = 0$. The solution is

$$x_\nu(t) = x_{0\nu} \frac{nG_\nu^\lambda}{\hbar\omega_\nu} [\cos \omega_\nu(t - T_P) - 1]. \quad (8)$$

Equation (8) shows that fast resonant pumping produces coherent oscillations of the nuclear displacements with amplitude $a_\nu = |\mathbf{x}_\nu| \equiv \frac{x_{0\nu}n|G_\nu^\lambda|}{\hbar\omega_\nu}$. In addition, the oscillations occur around an average displaced position $\mathbf{x}_\nu = -\text{sign}(G_\nu^\lambda)|\mathbf{x}_\nu|$, that can be positive or negative, depending on the sign of the X-*cph* coupling. If, on the other hand, the pump duration is comparable or larger than the phonon period then the average displaced position does not change while the amplitude of the oscillations reduces: $a_\nu = (n_\nu/n)|\mathbf{x}_\nu|$ with $n_\nu < n$. The “effective” densities $n_\nu = n_\nu(T_P)$ are decreasing functions of T_P which approach n for $T_P \ll T_\nu$ and zero for $T_P \gg T_\nu$. In fact, in the limit of very slow pumping the displacement $x_\nu(t) \approx \mathbf{x}_\nu$ becomes independent of time, consistently with the fact that the system is adiabatically driven toward a nonequilibrium steady-state.

Coherent modulation of the exciton energy

We now address how coherent phonons modify the exciton energy E^λ as measured in a transient optical experiments [44–48]. We are interested in probing the system at a time τ subsequent the phonon-induced dephasing of the electronic polarization [29, 57, 58] (typical time-scales are a few hundreds of femtoseconds). In this depolarized regime the inter-band elements of the density matrix vanish [59], i.e., $\rho_{\mathbf{k}vc} = 0$, and the system is in a nonequilibrium steady-state characterized by a density matrix $\rho = \rho_{\text{eq}} + \delta\rho$, with ρ_{eq} the ground state density matrix and $\delta\rho$ as in Eqs. (5). The quasi-particle Hamiltonian then reads $h_{\mathbf{k}}^{\text{qp}}(\tau) = h_{\mathbf{k}}^{\text{HSEX}}[\rho] + h_{\mathbf{k}}^{\text{Eh}}(\tau)$, where the first term is the HSEX Hamiltonian (which is a functional of the time-independent density matrix ρ) and the second term is the *time-dependent* Ehrenfest potential given by $h_{\mathbf{k}ij}^{\text{Eh}}(\tau) = \sum_\nu g_{ij}^\nu(\mathbf{k}) \frac{x_\nu(\tau)}{x_{0\nu}}$. The Ehrenfest potential arises from the photo-excited coherent motion of the nuclei and acts on the electrons with an intensity proportional to the bare *e-ph* couplings g [52].

For probe pulses shorter than the optical phonon periods the transient absorption spectrum can be obtained using the adiabatic approach of Ref. [60]. The absorption energies at time τ are the eigenvalues of the non-equilibrium BSE with Hamiltonian $H(\tau) = H + \delta H(\tau)$ with $\delta H(\tau) = \delta H^{\text{Eh}} + \delta K$. The change δK of the BSE kernel $K = \delta h^{\text{HSEX}}/\delta\rho$ in Eq. (4) is due to the pump-induced change of the density matrix [60]. The term δH^{Eh} does instead accounts for the renormalization of the quasi-particle energies caused by the Ehrenfest potential. It is responsible for the temporal modulation of the excitonic energies and reads

$$\delta H_{\mathbf{k}vc,\mathbf{k}'v'c'}^{\text{Eh}}(\tau) = \delta_{\mathbf{kk}'} \sum_{\nu} \frac{x_{\nu}(\tau)}{x_{0\nu}} [\delta_{vv'} g_{cc'}^{\nu}(\mathbf{k}) - \delta_{cc'} g_{v'v}^{\nu}(\mathbf{k})]. \quad (9)$$

For small excitation densities n , both δH^{Eh} and δK can be treated perturbatively, yielding the τ -dependent modification of the λ' excitonic energy

$$\begin{aligned} E^{\lambda'}(\tau) &= E^{\lambda'} + \sum_{\mathbf{kk}'cc'vv'} A_{\mathbf{k}vc}^{\lambda'*} [\delta H_{\mathbf{k}vc,\mathbf{k}'v'c'}(\tau)] A_{\mathbf{k}'v'c'}^{\lambda'} \\ &\equiv E^{\lambda'} + \delta E_K^{\lambda'} + \delta E^{\lambda'}(\tau). \end{aligned} \quad (10)$$

The constant shift $\delta E_K^{\lambda'}$ is due to δK , and it accounts for the renormalization caused by electronic correlation effects like band-gap renormalization [61–63], Pauli blocking [62, 64, 65] and excited-state screening [64–66]. The explicit evaluation of $\delta E_K^{\lambda'}$ has been the subject of several papers and is not discussed further here. The time-dependent shift $\delta E^{\lambda'}(\tau)$ origins from δH^{Eh} . Using the expression for $x_{\nu}(\tau)$ in Eq. (8), derived for $T_P \ll T_{\nu}$, we obtain that the modulation of the λ' exciton energy due to resonant pumping with the lowest exciton reads

$$\delta E^{\lambda'}(\tau) = n \sum_{\nu} \frac{G_{\nu}^{\lambda} G_{\nu}^{\lambda'}}{\hbar\omega_{\nu}} \times \left[\frac{n_{\nu}}{n} \cos \omega_{\nu}\tau - 1 \right], \quad (11)$$

that for $\lambda' = \lambda$ reduces to Eq. (2).

We conclude that the coupling with coherent phonons in resonantly excited materials is responsible for oscillations of the excitonic peak versus the impinging time τ of the probe [44–48]. The oscillation periods are dictated by the phonon frequencies and, for the lowest-energy exciton, the amplitude is proportional to the square of the X-cph coupling. Our result also predicts a likelihood of observing beatings when more phonons with different frequencies are strongly coupled to the exciton. This finding aligns with the outcomes of recent experiments in MoSe₂ [67].

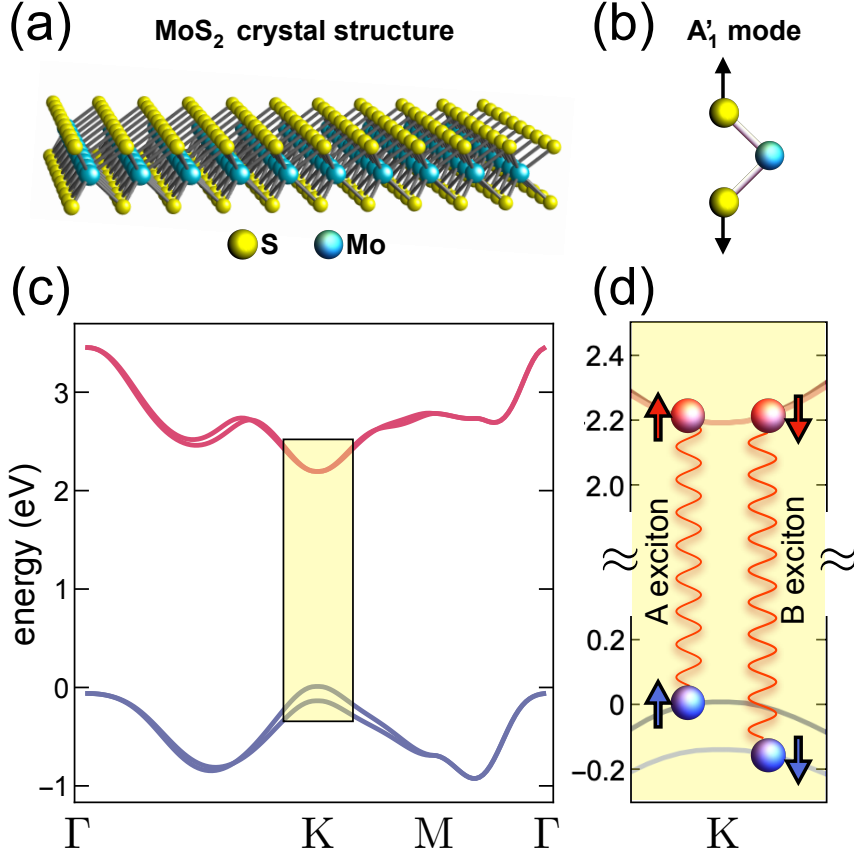


FIG. 1. (a) Crystal structure of a MoS₂ monolayer. (b) Geometrical representation of the A'_1 normal mode. (c) Electronic band structure. The yellow box at the K -point highlights the splitting due to spin-orbit interaction. (d) Pictorial view of the bands involved in the formation of A and B excitons.

Transient absorption in monolayer MoS₂

We validate our analytical findings through numerical simulations of the transient absorbance in monolayer MoS₂, see Fig. 1a. We use a tight-binding description of the band structure [68] and a Rytova-Keldysh potential for the screened interaction [69], and consider only the out-of-plane A'_1 normal mode. Recent experiments suggest that the photoexcited dynamics is dominated by such mode [44], see Fig. 1b. For the bare $e\text{-}ph$ coupling we use $g \approx \varepsilon g$ with dielectric constant $\varepsilon = 1$ – screening at vanishing momentum transfer is negligible in two-dimensional materials [69, 70]. The screened $e\text{-}ph$ couplings $g_{cc'}^{A'_1}$ and $g_{vv'}^{A'_1}$ have been evaluated with the **Quantum Espresso** package [71], and are displayed in Fig. 2. We propagate in time the electronic density matrix $\rho_{\mathbf{k}}(t)$ in the HSEX+Ehrenfest approximation

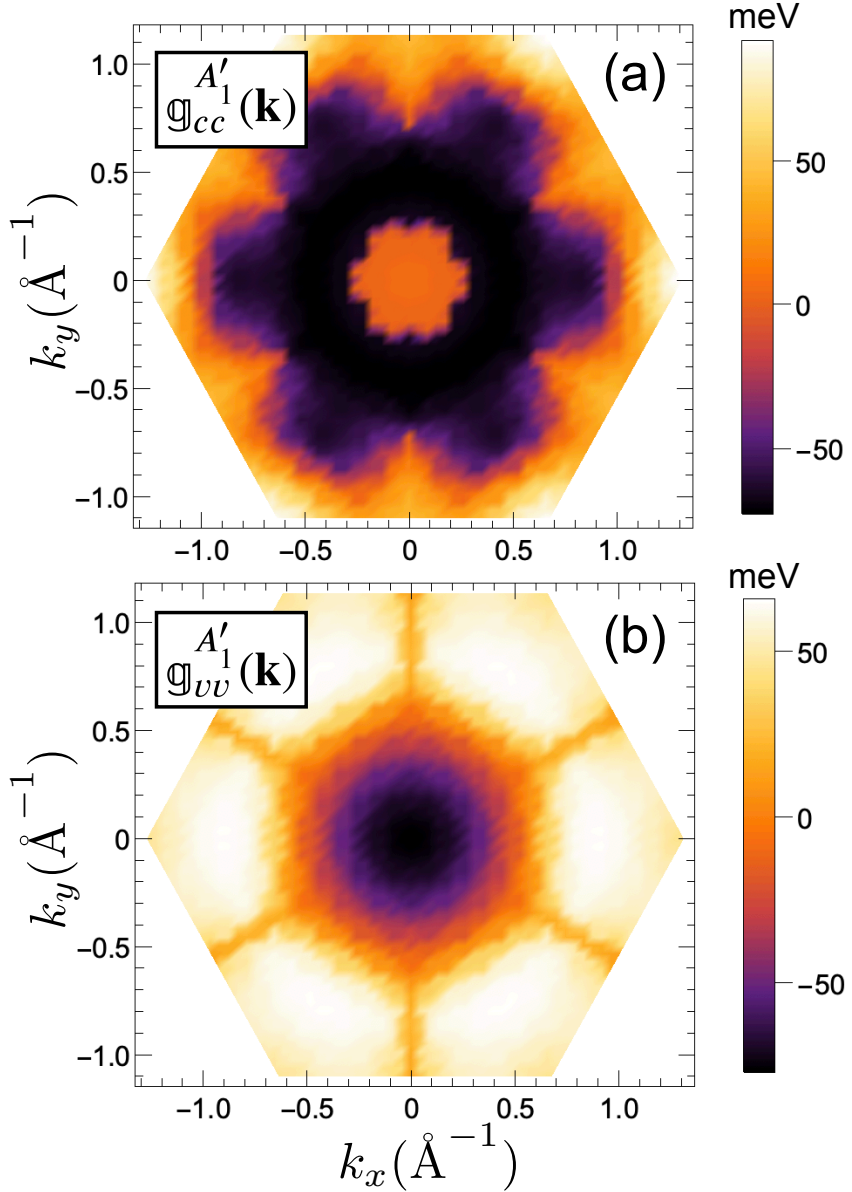


FIG. 2. Color plot of the coupling between the A'_1 optical phonon and electrons in the conduction (top) and valence (bottom) bands.

using the CHEERS code [72] (see Methods).

The dynamics is initiated by a linearly polarized pump pulse of duration $T_P = 20$ fs (much shorter than the optical period $T_{\nu=A'_1} \simeq 82$ fs) and energy $\hbar\omega_P = 1.9$ eV, which is in resonance with the A exciton, see Fig. 1c-d. The pump pulse does therefore induce a displacive excitation and we expect $n_{\nu=A'_1} \simeq n$. The excitation density for $t > T_P$ is found to be $n = 0.0013$, corresponding to a carrier density per unit area $n_x = n/A_{\text{MoS}_2} = 1.5 \times 10^{12} \text{ cm}^{-2}$

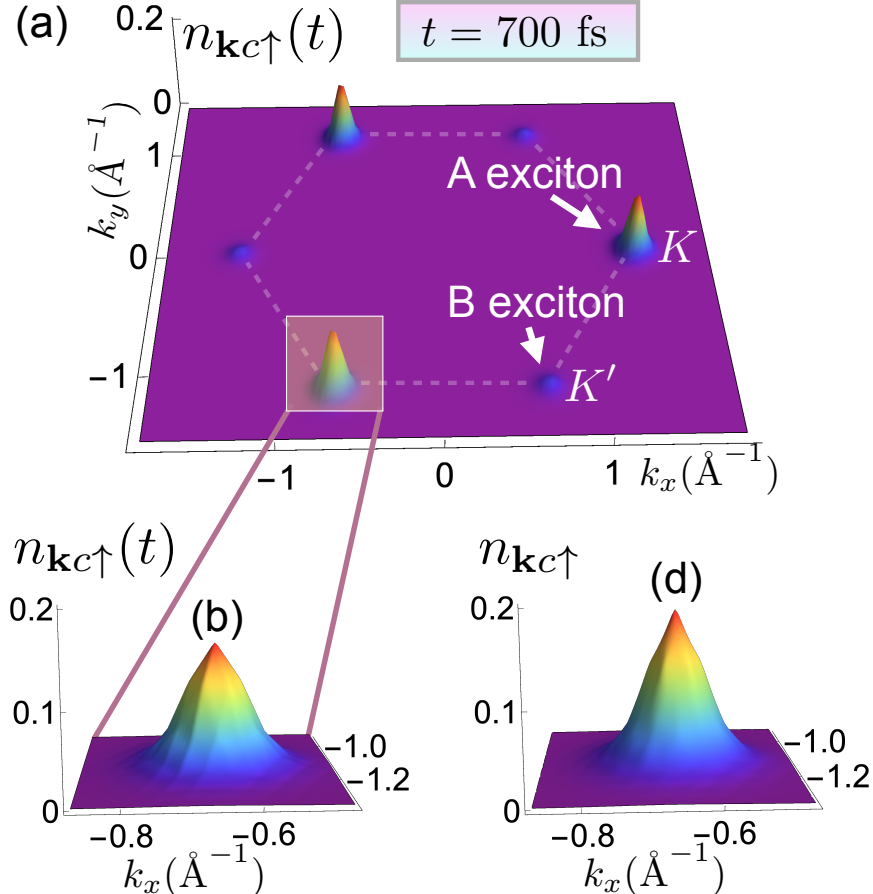


FIG. 3. (a) Plot of the density of spin-up electrons in the conduction band after 700 fs (depolarized regime), showing a predominance of the A exciton (K -point) over the B exciton (K' point). (b) Magnification of panel (a) around the K -point. (c) Analytic density of spin-up electrons in the conduction band around the K -point as obtained from Eq. (5a).

($A_{\text{MoS}_2} = 8.8 \text{ \AA}^2$ being the area of the unit cell). About 400 fs after the photoexcitation the system enters the depolarized regime with $\rho_{\mathbf{k}vc} \approx 0$ and $\rho_{\mathbf{kcc}'}$ and $\rho_{\mathbf{kvv}'}$ independent of time. In Fig. 3a we plot the occupations of spin-up electrons in the conduction band, i.e., $n_{\mathbf{k}c\uparrow}(t) = \rho_{\mathbf{k}c\uparrow c\uparrow}(t)$, at $t = 700 \text{ fs}$. In the spin-up sector the A and B excitons are located at the K and K' valleys respectively, see again Fig. 1c-d, whereas in the spin-down sector this configuration reverses [4]. In Fig. 3 we compare $n_{\mathbf{k}c\uparrow}(t)$ (panel b) with the analytic value $n_{\mathbf{k}c\uparrow} \equiv \delta\rho_{\mathbf{k}c\uparrow c\uparrow}$ from Eq. (5a) (panel c), which is proportional to the square modulus of the exciton wavefunction. The agreement is fairly good, thus confirming that resonant pumping generates a finite density of A excitons. The small discrepancy is due to the

finite duration of the pump, which prevents achieving a perfect resonant condition. As a result, a minimal contamination arises from the generation of a small density of B excitons, specifically observed in Fig. 3a at the K' valley.

To obtain the time-resolved absorption spectrum, we further impinge the system with a broadband probe pulse at different delay times τ . We then calculate for all times t the change in the density matrix $\Delta\rho(t, \tau) = \rho_{P+P}(t, \tau) - \rho_P(t)$, resulting from a simulation with pump and probe and a simulation with only the pump [60, 73]. The transient absorption spectrum is calculated as [60, 73]

$$\mathfrak{S}(\omega, \tau) = -2\omega \text{Im}[\mathbf{e}(\omega, \tau) \cdot \mathbf{d}(\omega, \tau)], \quad (12)$$

where $\mathbf{e}(\omega, \tau)$ is the Fourier transform of the probe field and $\mathbf{d}(\omega, \tau)$ is the Fourier transform of the probe-induced dipole moment $\mathbf{d}(t, \tau)$. The latter is related to the change of the density matrix via $\mathbf{d}(t, \tau) = \sum_{\mathbf{k}} \text{Tr}[\mathbf{d}_{\mathbf{k}} \Delta\rho_{\mathbf{k}}(t, \tau)]$, where $\mathbf{d}_{\mathbf{k}}$ is the dipole transition matrix. Equation (12) generalizes the equilibrium absorption spectrum to out-of-equilibrium conditions. In the absence of pump fields (equilibrium condition) we have $\mathbf{d}(\omega, \tau) = \text{Tr}[\chi(\omega) \cdot \mathbf{e}(\omega)]$ independent of τ , with $\chi(\omega)$ the dipole-dipole response function, and $\mathfrak{S}(\omega, \tau)$ reduces to equilibrium absorption spectrum [60, 74].

We have conducted simulations for several equidistant delay times $\tau_n = n\Delta_{\tau}$, encompassing approximately 100 distinct values spanning a relatively long time-window (~ 1 ps). The dependence of the spectrum on τ originates from the time-dependent HSEX+Ehrenfest potential: the specific timing at which the probe interacts with the system determines the value of $h^{qp}(\tau)$, resulting in different frequencies for $\Delta\rho_{\mathbf{k}vc}(t, \tau)$.

In Fig. 4a we display the logarithmic plot of $\mathfrak{S}(\omega, \tau)$ for energies $\hbar\omega$ up to a few meV below the exciton energy $E^A \simeq 1.9$ eV. The spectrum changes wildly until the pump-induced polarization is sizable (coherent regime), i.e., up to $\tau \simeq 400$ fs. Both the position and the amplitude of the excitonic peak oscillate with a period of $T^A = 2\pi/E^A \sim 2.2$ fs. In our simulations, however, the system is probed every $\Delta_{\tau} = 7.75$ fs, preventing us to resolve the faster time-scale T^A . Instead, an artificial period $T \sim 31$ fs [corresponding to the matching condition $T \sim pT^A \sim q\Delta_{\tau}$ with p and q prime numbers] is observed.

The position $E^A(\tau)$ of the A exciton energy, calculated as the maximum $\max_{\omega} \mathfrak{S}(\omega, \tau)$, is shown in Fig. 4b (blue dots). The exciton is initially blue-shifted with respect to its equilibrium value. This blue-shift undergoes relaxation within about 200 fs, eventually

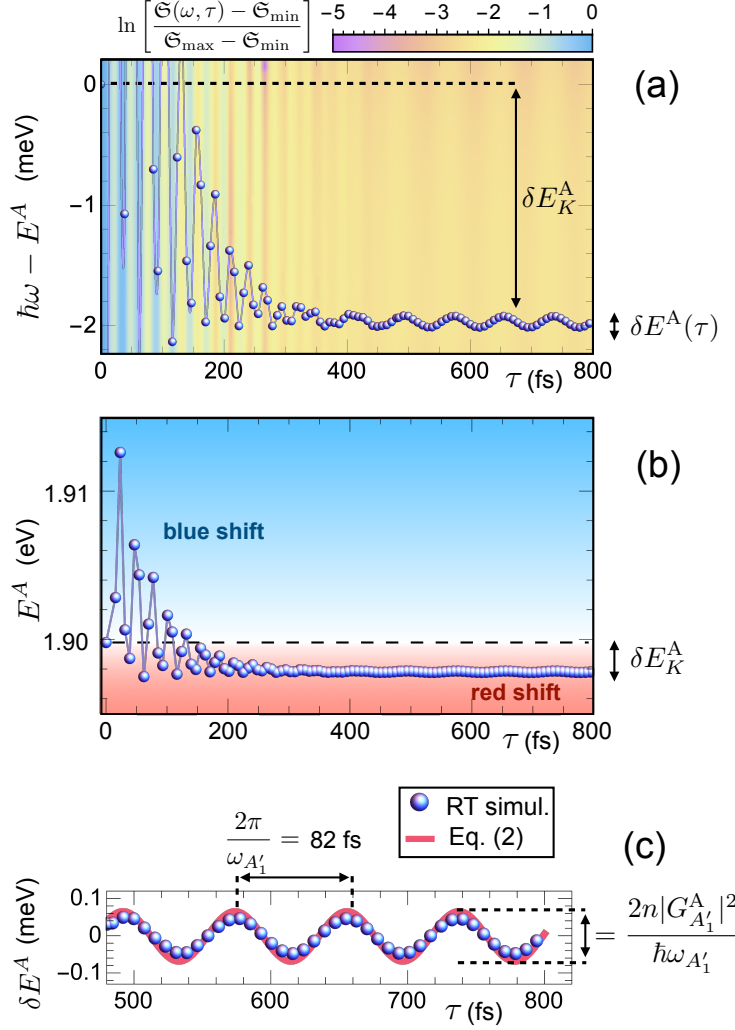


FIG. 4. (a) Color plot of the logarithmic transient absorption spectrum $\ln \left[\frac{\mathfrak{S}(\omega, \tau) - \mathfrak{S}_{\min}}{\mathfrak{S}_{\max} - \mathfrak{S}_{\min}} \right]$ versus energy (vertical axis) and delay (horizontal axis). Here \mathfrak{S}_{\min} and \mathfrak{S}_{\max} denote the minimum and maximum values of $\mathfrak{S}(\omega, \tau)$ in the displayed region. Blue dots indicate the position of the maxima of $\mathfrak{S}(\omega, \tau)$ for different delays. The electronic red-shift δE_K^A and the phonon-induced coherent modulation $\delta E_A^A(\tau)$ are also indicated. (b) Temporal evolution of the exciton energy $E_A^A(\tau)$ as a function of the pump-probe delay τ . The reference equilibrium value $E_A^A(0) = 1.9$ eV is shown as a dashed line, while blue and red backgrounds are used visualize blue- and red-shift regions respectively. (c) Comparison of the position of the exciton peak as obtained from the real-time (RT) simulations of panel (a) (blue dots) and the analytic formula in Eq. (2) (red curve).

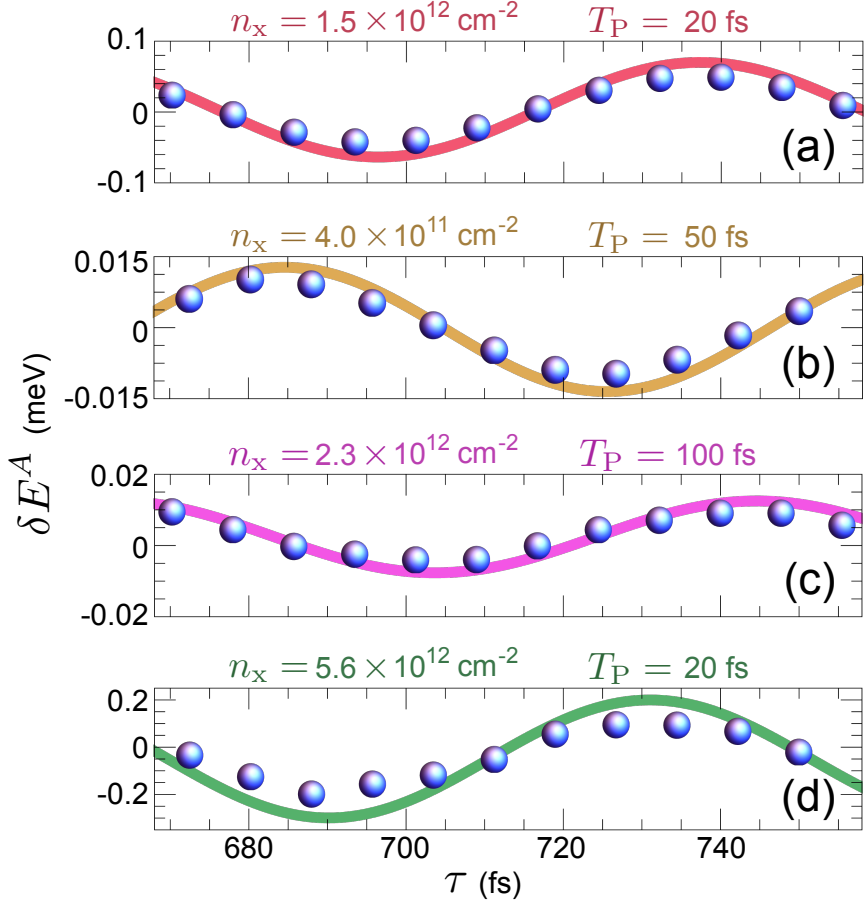


FIG. 5. Comparison of the oscillations of the exciton peak δE^A from RT simulations (blue dots) with the analytic result of Eq. (2) (solid curves) for different pump durations T_P and excitation densities n_x . Panel a: $T_P = 20$ fs, $n_x = 1.5 \times 10^{12} \text{ cm}^{-2}$ ($n_{A'_1} = n$); Panel b: $T_P = 50$ fs, $n_x = 4.0 \times 10^{11} \text{ cm}^{-2}$ ($n_{A'_1} = 0.71n$); Panel c: $T_P = 100$ fs, $n_x = 2.3 \times 10^{12} \text{ cm}^{-2}$ ($n_{A'_1} = 0.1n$); Panel d: $T_P = 20$ fs, $n_x = 5.6 \times 10^{12} \text{ cm}^{-2}$ ($n_{A'_1} = n$);

transitioning into a stable red-shift $\delta E_K^A \approx 2$ meV due to electronic mechanisms (change of the BSE kernel), see Eq. (10). The decay time of this transition is governed by the polarization lifetime which, in turns, depends strongly on the excitation density and it can vary from hundreds of femtoseconds to picoseconds. Our observations align closely with the work by Calati et al. [75], where a similar blue-to-red transition has been reported in resonantly excited WS₂. Entering the depolarized (or incoherent) regime the wild oscillations gradually attenuate, and the intensity of the signal begins to oscillate at the phonon frequency $\omega_{A'_1}$, see Fig. 4a. For $\tau > 400$ fs, the exciton position $\delta E^A(\tau)$ features oscillations at the very same

frequency around the red-shifted value $E^A + \delta E_K^A$, in qualitative agreement with Eq. (10) and Eq. (2).

Inspecting the amplitude of the oscillations, we also appreciate an excellent quantitative agreement, see Fig. 4c. The red curve is the plot of Eq. (2) with $n_{A'_1} = n$ (displacive excitation) and $n = 0.0013$ the excitation density created by the pump. The value of the $X\text{-}cph$ coupling is $G_{A'_1}^A \approx 50$ meV, implying that resonant pumping with the A exciton brings the MoS₂ monolayer toward a nonequilibrium steady-state characterized by a vertical compression of the sulphur atoms ($x_{A'_1} < 0$).

As the analytic formula in Eq. (2) has been derived in the limit of low excitation density and short pump duration (displacive regime), we have explored the extent to which its applicability is affected when the photoexcitation deviates from these conditions, see Fig. 5. To facilitate comparisons a τ -slice of Fig. 4c is shown in panel a. In panel b we consider longer pump pulses with duration $T_P = 50$ fs, while still maintaining a small excitation density $n_x = 4 \times 10^{11}$ cm⁻². In this case a correction due to the effective density $n_{A'_1}$ must be introduced [see Eqs.(2) and (8)] since the photoexcitation is no longer displacive. The value $n_{A'_1}/n = a_{A'_1}/|x_{A'_1}| = 0.71$ is extracted by taking the ratio between the amplitude of the oscillations $a_{A'_1}$ of the A'_1 mode as obtained from the numerical simulation and the analytic value $|x_{A'_1}| = \frac{x_{0A'_1} n |G_{A'_1}^\lambda|}{\hbar \omega_{A'_1}}$. Remarkably, the validity of the analytic formula extends well beyond the initially defined applicability region. In panel c we consider a very long pump $T_P = 100$ fs and a relatively high excitation density $n_x = 2.3 \times 10^{12}$ cm⁻². Applying the correction $n_{A'_1}/n = 0.10$, the agreement between the simulated and predicted excitonic oscillations is still reasonably good. Further increasing the excitation density, $n_x = 5.6 \times 10^{12}$ cm⁻², the agreement begins to deteriorate, even within the displacive regime, see panel d, where $n_{A'_1}/n = 1$.

III. DISCUSSION

We present the many-body theory of the interaction between resonantly pumped excitons and coherent phonons, and derive the expression of the $X\text{-}cph$ coupling. The magnitude of this coupling can exceed that of the $X\text{-}ph$ coupling in three dimensions, given that the bare (screened) $e\text{-}ph$ matrix elements are used to calculate the former (latter). We also derive a readily applicable formula to quantify the modulations of the excitonic energies in

resonantly pumped materials [44–48]. The accuracy of the formula is demonstrated through comparisons with model simulations of transient absorption in a MoS₂ monolayer. Our findings provide a straightforward means to directly extract the value of the X-*cph* coupling, along with accurately determining the magnitude of the excitation density.

IV. METHODS

Real-time HSEX + Ehrenfest method

We describe in detail the method that we use to propagate in time the electronic one-particle density matrix $\rho_{\mathbf{k}ij}$ together with the phonon displacement $x_\nu(t)$ and momentum $p_\nu(t)$. Here \mathbf{k} denotes the cristal momentum, i, j the spin-band indices that can be valence (v) or conduction (c), while ν denotes the phonon mode. Our method is based on the Hartree plus statically screened exchange (HSEX) plus Ehrenfest approximation of many-body theory. The coupled equations of motion to be propagated in time read [52, 55]

$$\begin{aligned} i \frac{d}{dt} \rho_{\mathbf{k}ij}(t) &= [h_{\mathbf{k}}^{\text{qp}}(t), \rho_{\mathbf{k}}(t)]_{ij} + I_{\mathbf{k}ij}^{\text{coll}}(t), \\ p_\nu(t) &= -\omega_\nu x_\nu(t) - \sum_{\mathbf{k}, ij} g_{ij}^\nu(\mathbf{k}, 0) \rho_{\mathbf{k}ji}(t) \\ \frac{d}{dt} x_\nu(t) &= \omega_\nu p_\nu(t). \end{aligned} \quad (13)$$

In Eq. (13) h^{qp} is the quasi-particle hamiltonian given by

$$\begin{aligned} h_{\mathbf{k}ij}^{\text{qp}}(t) &= h_{\mathbf{k}ij}^{\text{HSEX}}(t) + h_{\mathbf{k}ij}^{\text{Eh}}(t) \\ &= \delta_{ij} \epsilon_{\mathbf{k}i} + \sum_{\mathbf{k}_1 mn} (V_{imnj}^{\mathbf{0}\mathbf{k}\mathbf{k}_1} - V_{imjn}^{(\mathbf{k}-\mathbf{k}_1)\mathbf{k}\mathbf{k}_1}) \delta \rho_{\mathbf{k}_1 nm}(t) + \mathbf{E}(t) \cdot \mathbf{d}_{\mathbf{k}ij} + \sum_\nu x_\nu(t) g_{ij}^\nu(\mathbf{k}) \end{aligned} \quad (14)$$

This hamiltonian accounts for (i) the electron kinetic energy (via the band structure $\epsilon_{\mathbf{k}i}$), (ii) the interaction with the external laser pulses $\mathbf{E}(t)$ (via the dipole matrix elements $\mathbf{d}_{\mathbf{k}ij}$), (iii) the HSEX self-energy (via the electron-electron interaction $V_{imjn}^{\mathbf{q}\mathbf{k}\mathbf{k}'}$), and (iv) the Ehrenfest potential describing the coupling of electrons with the nuclear displacements (via the bare electron-phonon coupling $g_{ij}^\nu(\mathbf{k}) \equiv g_{ij}^\nu(\mathbf{k}, 0)$ at vanishing momentum transfer). The presence of the HSEX and Ehrenfest potentials guarantees that strong excitonic effects and the coupling of excitons to coherent phonons are included in the photoexcited dynamics. The SEX interaction is modeled by the Rytova-Keldysh potential [69, 76] (see also below) which has demonstrated remarkable accuracy in reproducing excitonic binding energies in 2D materials [2, 64, 77]. The evaluation of the Ehrenfest potential and the effective forces acting on the nuclei require only the intra-band electron-phonon couplings $g_{ii}^\nu(\mathbf{k})$ at $\mathbf{q} = 0$ [52]. The couplings g can be evaluated according to

$$g_{ii}^\nu(\mathbf{k}) = \sqrt{\frac{\hbar}{2M\omega_\nu}} \frac{\partial E_{\mathbf{k}i}}{\partial x_\nu}, \quad (15)$$

where $E_{\mathbf{k}i}$ is the Kohn-Sham energy of the i -th band at momentum \mathbf{k} , $\omega_\nu = \omega_\nu(\mathbf{q} = 0)$ is the

frequency of mode ν at the Γ point, and x_ν denotes the ion displacement along the phonon mode ν with momentum $\mathbf{q} = 0$.

In MoS₂ monolayers the mostly coupled phonon is the out-of-plane A'_1 optical mode [44]. Therefore, only this specific normal mode has been included in our simulations. The last term in the equation of motion for ρ is the collision integral $I^{\text{coll}}(t)$, that incorporates dynamical correlation effects responsible for, e.g., inelastic quasi-particle scattering, decoherence and dynamical screening [59, 78–80]. At low and moderate excitation densities the dominant contribution to the collision integral stems from electron-phonon scattering which drives the system toward a depolarized regime characterized by the disappearance of valence-conduction elements $\rho_{\mathbf{k},vc}$ of the density matrix [54, 55, 59]. For this reason all matrix elements of the collision integral are neglected, except for the valence-conduction ones that we approximate as $I_{\mathbf{k},vc}^{\text{coll}}(t) = -2i\gamma\rho_{\mathbf{k},cv}(t)$. Here $\hbar/\gamma = 250$ fs is the dephasing time of the electronic polarization experimentally observed in MoS₂ at low temperature [58]. The three coupled equations of motion in Eq. (13) are numerically integrated by using a 4th order Runge-Kutta solver with a time step $\Delta t = 0.1$ fs as implemented in the CHEERS code [72].

For our simulations in MoS₂ we select as active space the two highest valence and the two lowest conduction spin-bands. Therefore the spin-band index i can take the 4 values $i = \{(v \uparrow), (v \downarrow), (c \uparrow), (c \downarrow)\}$. In this way spin-orbit effects responsible for the energy splitting between A and B excitons are included.

From a knowledge of the electronic density matrix we can evaluate the momentum resolved carrier populations $n_{\mathbf{k}i}(t)$ according to

$$n_{\mathbf{k}i}(t) = \rho_{\mathbf{k}ii}(t). \quad (16)$$

Using the off-diagonal elements of ρ we can also calculate the probe-induced dipole moment according to

$$\mathbf{d}(t) = \sum_{\mathbf{k}} \mathbf{d}_{\mathbf{k}}(t), \quad \mathbf{d}_{\mathbf{k}}(t) = \sum_{ij} \rho_{\mathbf{k}ij}(t) \mathbf{d}_{\mathbf{k}ji} \quad (17)$$

Modelization of the MoS₂ monolayer

We calculate the spin-orbit dependent band structure of a MoS₂ monolayer from the tight-binding parametrization provided in Ref. [68] that gives low-energy bands $\epsilon_{\mathbf{k}i}$ in very good agreement with DFT calculations. The conduction bands are rigidly shifted-up by 0.6 eV, to match the quasiparticle bandgap measured in ARPES experiments [81]. For the RT simulations we consider

the two highest valence bands and the two lowest conduction bands as our active space. The Coulomb integral $V_{imjn}^{\mathbf{qkk}'}$ accounting for the scattering amplitude of two electrons in bands j and n with quasimomenta $\mathbf{k}' + \mathbf{q}$ and $\mathbf{k} - \mathbf{q}$ to end up in bands m and i with quasimomenta \mathbf{k}' and \mathbf{k} respectively is calculated according to $V_{imjn}^{\mathbf{qkk}'} = v_q(\mathbf{U}_{\mathbf{k}i}^\dagger \cdot \mathbf{U}_{\mathbf{k}-\mathbf{q}n})(\mathbf{U}_{\mathbf{k}'m}^\dagger \cdot \mathbf{U}_{\mathbf{k}'+\mathbf{q}j})$ [82], where $\mathbf{U}_{\mathbf{k}i}$ are the eigenvectors of the Bloch Hamiltonian $H_{\mathbf{k}}$ and v_q is the Rytova-Keldysh potential [69, 76] in momentum space, i.e.

$$v_q = \frac{2\pi}{\epsilon q(1 + r_0 q)}. \quad (18)$$

In the above equation $q = |\mathbf{q}|$, $r_0 = 33.875 \text{ \AA}/\epsilon$ [82], and $\epsilon = 2.5$ is the dielectric constant of a typical substrate (the topstrate is supposed to be air). The regularization of the diverging value of v_q at the Γ point is expressed as [83, 84] $v(0) \rightarrow \frac{1}{\Omega} \int_{\Omega} d\mathbf{q} v(q)$. Here Ω represents a 2D domain around $\mathbf{q} = 0$ of linear dimension determined by the discretization step of the first Brillouin zone. In this study, the first Brillouin zone has been discretized using a C_{6v} -symmetric grid comprising 3072 \mathbf{k} -points. In semiconductor materials the Coulomb integrals that do not conserve the number of valence and conduction electrons are typically negligible [85] and have been excluded from our calculations. Finally the dipole matrix elements are evaluated according to [64, 86]

$$\mathbf{d}_{\mathbf{k}ij} = \frac{1}{i} \frac{1}{\epsilon_{\mathbf{k}i} - \epsilon_{\mathbf{k}j}} \mathbf{U}_{\mathbf{k}i}^\dagger \cdot \partial_{\mathbf{k}} H_{\mathbf{k}} \cdot \mathbf{U}_{\mathbf{k}j}. \quad (19)$$

Concerning the phonon input, the electron-phonon coupling in Eq. (15) are obtained by displacing manually the ions along the phonon eigenvector directions (with equilibrium lattice constant $a = 3.12 \text{ \AA}$) and by calculating the corresponding difference in the band structure. This procedure is very accurate for the out-of-plane optical mode A'_1 [87]. The Kohn-Sham energies $E_{\mathbf{k}i}$ for a given displaced configuration are calculated with Quantum ESPRESSO using LDA in a 24×24 grid. The phonon frequencies ω_ν are evaluated within the same grid.

Data availability

The datasets used for this study are available from the corresponding authors upon request.

Code availability

The code used for this study is available from the corresponding authors upon request.

Acknowledgments

The Authors acknowledge funding from Ministero Università e Ricerca PRIN under grant agreement No. 2022WZ8LME, from the INFN TIME2QUEST project, from the European Research Council MSCA-ITN TIMES under grant agreement 101118915, and from Tor Vergata University through Project TESLA.

Author contributions

KW performed the DFT ab-initio calculations of the electron-phonon couplings. EP and GS contributed equally to this work and to the preparation of this manuscript.

Competing interests

The Authors declare no competing interests.

References

- [1] Diana Y. Qiu, Felipe H. da Jornada, and Steven G. Louie. Optical spectrum of mos₂: Many-body effects and diversity of exciton states. *Phys. Rev. Lett.*, 111:216805, Nov 2013. URL <https://link.aps.org/doi/10.1103/PhysRevLett.111.216805>.
- [2] Alexey Chernikov, Timothy C. Berkelbach, Heather M. Hill, Albert Rigosi, Yilei Li, Ozgur Burak Aslan, David R. Reichman, Mark S. Hybertsen, and Tony F. Heinz. Exciton binding energy and nonhydrogenic rydberg series in monolayer ws₂. *Phys. Rev. Lett.*, 113:076802, Aug 2014. URL <https://link.aps.org/doi/10.1103/PhysRevLett.113.076802>.
- [3] Keliang He, Nardeep Kumar, Liang Zhao, Zefang Wang, Kin Fai Mak, Hui Zhao, and Jie Shan. Tightly bound excitons in monolayer wse₂. *Phys. Rev. Lett.*, 113:026803, Jul 2014. URL <https://link.aps.org/doi/10.1103/PhysRevLett.113.026803>.
- [4] Gang Wang, Alexey Chernikov, Mikhail M. Glazov, Tony F. Heinz, Xavier Marie, Thierry Amand, and Bernhard Urbaszek. Colloquium: Excitons in atomically thin transition metal dichalcogenides. *Rev. Mod. Phys.*, 90:021001, Apr 2018. URL <https://link.aps.org/doi/10.1103/RevModPhys.90.021001>.
- [5] Samuel D. Stranks, Victor M. Burlakov, Tomas Leijtens, James M. Ball, Alain Goriely, and Henry J. Snaith. Recombination kinetics in organic-inorganic perovskites: Excitons, free charge, and subgap states. *Phys. Rev. Appl.*, 2:034007, Sep 2014. doi:10.1103/PhysRevApplied.2.034007. URL <https://link.aps.org/doi/10.1103/PhysRevApplied.2.034007>.
- [6] Michal Baranowski and Paulina Plochocka. Excitons in metal-halide perovskites. *Advanced Energy Materials*, 10(26):1903659, 2020. doi:<https://doi.org/10.1002/aenm.201903659>. URL <https://onlinelibrary.wiley.com/doi/abs/10.1002/aenm.201903659>.
- [7] Michael A. Becker, Roman Vaxenburg, Georgian Nedelcu, Peter C. Sercel, Andrew Shabaev, Michael J. Mehl, John G. Michopoulos, Samuel G. Lambrakos, Noam Bernstein, John L. Lyons, Thilo Stöferle, Rainer F. Mahrt, Maksym V. Kovalenko, David J. Norris, Gabriele Rainò, and Alexander L. Efros. Bright triplet excitons in caesium lead halide perovskites. *Nature*, 553(7687):189–193, 2018. doi:10.1038/nature25147. URL <https://doi.org/10.1038/nature25147>.

[nature25147](#).

- [8] Wei Wei, Ying Dai, Baibiao Huang, and Timo Jacob. Many-body effects in silicene, silicane, germanene and germanane. *Phys. Chem. Chem. Phys.*, 15:8789–8794, 2013. doi: 10.1039/C3CP51078F. URL <http://dx.doi.org/10.1039/C3CP51078F>.
- [9] Matthew N. Brunetti, Oleg L. Berman, and Roman Ya. Kezerašvili. Optical properties of anisotropic excitons in phosphorene. *Phys. Rev. B*, 100:155433, Oct 2019. doi: 10.1103/PhysRevB.100.155433. URL <https://link.aps.org/doi/10.1103/PhysRevB.100.155433>.
- [10] Matthew N. Brunetti, Oleg L. Berman, and Roman Ya. Kezerašvili. Optical properties of excitons in buckled two-dimensional materials in an external electric field. *Phys. Rev. B*, 98: 125406, Sep 2018. doi:10.1103/PhysRevB.98.125406. URL <https://link.aps.org/doi/10.1103/PhysRevB.98.125406>.
- [11] S. Latini, T. Olsen, and K. S. Thygesen. Excitons in van der waals heterostructures: The important role of dielectric screening. *Phys. Rev. B*, 92:245123, Dec 2015. doi: 10.1103/PhysRevB.92.245123. URL <https://link.aps.org/doi/10.1103/PhysRevB.92.245123>.
- [12] Ying Jiang, Shula Chen, Weihao Zheng, Biyuan Zheng, and Anlian Pan. Interlayer exciton formation, relaxation, and transport in tmd van der waals heterostructures. *Light: Science & Applications*, 10(1):72, 2021. doi:10.1038/s41377-021-00500-1. URL <https://doi.org/10.1038/s41377-021-00500-1>.
- [13] Kha Tran, Galan Moody, Fengcheng Wu, Xiaobo Lu, Junho Choi, Kyounghwan Kim, Amritesh Rai, Daniel A. Sanchez, Jiamin Quan, Akshay Singh, Jacob Embley, André Zepeda, Marshall Campbell, Travis Autry, Takashi Taniguchi, Kenji Watanabe, Nanshu Lu, Sanjay K. Banerjee, Kevin L. Silverman, Suenne Kim, Emanuel Tutuc, Li Yang, Allan H. MacDonald, and Xiaoqin Li. Evidence for moiréexcitons in van der waals heterostructures. *Nature*, 567(7746):71–75, 2019. doi:10.1038/s41586-019-0975-z. URL <https://doi.org/10.1038/s41586-019-0975-z>.
- [14] Qing Hua Wang, Kourosh Kalantar-Zadeh, Andras Kis, Jonathan N. Coleman, and Michael S. Strano. Electronics and optoelectronics of two-dimensional transition metal dichalcogenides. *Nature Nanotechnology*, 7(11):699–712, Nov 2012. URL <https://doi.org/10.1038/nnano.2012.193>.

- [15] Kin Fai Mak and Jie Shan. Photonics and optoelectronics of 2d semiconductor transition metal dichalcogenides. *Nature Photonics*, 10(4):216–226, Apr 2016. URL <https://doi.org/10.1038/nphoton.2015.282>.
- [16] Thomas Mueller and Ermin Malic. Exciton physics and device application of two-dimensional transition metal dichalcogenide semiconductors. *npj 2D Materials and Applications*, 2(1):29, 2018. doi:10.1038/s41699-018-0074-2. URL <https://doi.org/10.1038/s41699-018-0074-2>.
- [17] Daniel N. Congreve, Jiye Lee, Nicholas J. Thompson, Eric Hontz, Shane R. Yost, Philip D. Reusswig, Matthias E. Bahlke, Sebastian Reineke, Troy Van Voorhis, and Marc A. Baldo. External quantum efficiency above 100% in a singlet-exciton-fission-based organic photovoltaic cell. *Science*, 340(6130):334–337, 2013. doi:10.1126/science.1232994. URL <https://www.science.org/doi/abs/10.1126/science.1232994>.
- [18] Askat E. Jailaubekov, Adam P. Willard, John R. Tritsch, Wai-Lun Chan, Na Sai, Raluca Gearba, Loren G. Kaake, Kenrick J. Williams, Kevin Leung, Peter J. Rossky, and X-Y. Zhu. Hot charge-transfer excitons set the time limit for charge separation at donor/acceptor interfaces in organic photovoltaics. *Nature Materials*, 12(1):66–73, 2013. doi:10.1038/nmat3500. URL <https://doi.org/10.1038/nmat3500>.
- [19] Marco Bernardi, Maurizia Palummo, and Jeffrey C. Grossman. Extraordinary sunlight absorption and one nanometer thick photovoltaics using two-dimensional monolayer materials. *Nano Letters*, 13(8):3664–3670, 2013. doi:10.1021/nl401544y. URL <https://doi.org/10.1021/nl401544y>. PMID: 23750910.
- [20] Hui Wang, Wenxiu Liu, Xin He, Peng Zhang, Xiaodong Zhang, and Yi Xie. An excitonic perspective on low-dimensional semiconductors for photocatalysis. *Journal of the American Chemical Society*, 142(33):14007–14022, 2020. doi:10.1021/jacs.0c06966. URL <https://doi.org/10.1021/jacs.0c06966>. PMID: 32702981.
- [21] Yunyang Qian, Dandan Li, Yulan Han, and Hai-Long Jiang. Photocatalytic molecular oxygen activation by regulating excitonic effects in covalent organic frameworks. *Journal of the American Chemical Society*, 142(49):20763–20771, 2020. doi:10.1021/jacs.0c09727. URL <https://doi.org/10.1021/jacs.0c09727>. PMID: 33226795.
- [22] Hui Wang, Xianshun Sun, Dandan Li, Xiaodong Zhang, Shichuan Chen, Wei Shao, Yupeng Tian, and Yi Xie. Boosting hot-electron generation: Exciton dissociation at the order-disorder interfaces in polymeric photocatalysts. *Journal of the American Chemical Society*, 139(6):

- 2468–2473, 2017. doi:10.1021/jacs.6b12878. URL <https://doi.org/10.1021/jacs.6b12878>. PMID: 28102077.
- [23] Feliciano Giustino. Electron-phonon interactions from first principles. *Rev. Mod. Phys.*, 89:015003, Feb 2017. doi:10.1103/RevModPhys.89.015003. URL <https://link.aps.org/doi/10.1103/RevModPhys.89.015003>.
- [24] Galan Moody, Chandriker Kavir Dass, Kai Hao, Chang-Hsiao Chen, Lain-Jong Li, Akshay Singh, Kha Tran, Genevieve Clark, Xiaodong Xu, Gunnar Berghäuser, Ermin Malic, Andreas Knorr, and Xiaoqin Li. Intrinsic homogeneous linewidth and broadening mechanisms of excitons in monolayer transition metal dichalcogenides. *Nature Communications*, 6(1):8315, 2015. URL <https://doi.org/10.1038/ncomms9315>.
- [25] Colin M. Chow, Hongyi Yu, Aaron M. Jones, John R. Schaibley, Michael Koehler, David G. Mandrus, R. Merlin, Wang Yao, and Xiaodong Xu. Phonon-assisted oscillatory exciton dynamics in monolayer mose2. *npj 2D Materials and Applications*, 1(1):33, 2017. doi:10.1038/s41699-017-0035-1. URL <https://doi.org/10.1038/s41699-017-0035-1>.
- [26] Thibault Sohier, Evgeniy Ponomarev, Marco Gibertini, Helmuth Berger, Nicola Marzari, Nicolas Ubrig, and Alberto F. Morpurgo. Enhanced electron-phonon interaction in multi-valley materials. *Phys. Rev. X*, 9:031019, Aug 2019. doi:10.1103/PhysRevX.9.031019. URL <https://link.aps.org/doi/10.1103/PhysRevX.9.031019>.
- [27] Andrea Marini. Ab initio finite-temperature excitons. *Phys. Rev. Lett.*, 101:106405, Sep 2008. doi:10.1103/PhysRevLett.101.106405. URL <https://link.aps.org/doi/10.1103/PhysRevLett.101.106405>.
- [28] Tianlun Allan Huang, Marios Zacharias, D. Kirk Lewis, Feliciano Giustino, and Sahar Sharifzadeh. Exciton-phonon interactions in monolayer germanium selenide from first principles. *The Journal of Physical Chemistry Letters*, 12(15):3802–3808, 2021. doi:10.1021/acs.jpclett.1c00264. URL <https://doi.org/10.1021/acs.jpclett.1c00264>. PMID: 33848154.
- [29] P. Dey, J. Paul, Z. Wang, C. E. Stevens, C. Liu, A. H. Romero, J. Shan, D. J. Hilton, and D. Karaiskaj. Optical coherence in atomic-monolayer transition-metal dichalcogenides limited by electron-phonon interactions. *Phys. Rev. Lett.*, 116:127402, Mar 2016. doi:10.1103/PhysRevLett.116.127402. URL <https://link.aps.org/doi/10.1103/PhysRevLett.116.127402>.

- [30] F. Cadiz, E. Courtade, C. Robert, G. Wang, Y. Shen, H. Cai, T. Taniguchi, K. Watanabe, H. Carrere, D. Lagarde, M. Manca, T. Amand, P. Renucci, S. Tongay, X. Marie, and B. Urbaszek. Excitonic linewidth approaching the homogeneous limit in mos₂-based van der waals heterostructures. *Phys. Rev. X*, 7:021026, May 2017. doi:10.1103/PhysRevX.7.021026. URL <https://link.aps.org/doi/10.1103/PhysRevX.7.021026>.
- [31] P. Dey, J. Paul, Z. Wang, C. E. Stevens, C. Liu, A. H. Romero, J. Shan, D. J. Hilton, and D. Karaiskaj. Optical coherence in atomic-monolayer transition-metal dichalcogenides limited by electron-phonon interactions. *Phys. Rev. Lett.*, 116:127402, Mar 2016. doi:10.1103/PhysRevLett.116.127402. URL <https://link.aps.org/doi/10.1103/PhysRevLett.116.127402>.
- [32] Koloman Wagner, Jonas Zipfel, Roberto Rosati, Edith Wietek, Jonas D. Ziegler, Samuel Brem, Raül Perea-Causín, Takashi Taniguchi, Kenji Watanabe, Mikhail M. Glazov, Ermin Malic, and Alexey Chernikov. Nonclassical exciton diffusion in monolayer wse₂. *Phys. Rev. Lett.*, 127:076801, Aug 2021. doi:10.1103/PhysRevLett.127.076801. URL <https://link.aps.org/doi/10.1103/PhysRevLett.127.076801>.
- [33] Jonas D. Ziegler, Jonas Zipfel, Barbara Meisinger, Matan Menahem, Xiangzhou Zhu, Takashi Taniguchi, Kenji Watanabe, Omer Yaffe, David A. Egger, and Alexey Chernikov. Fast and anomalous exciton diffusion in two-dimensional hybrid perovskites. *Nano Letters*, 20(9): 6674–6681, 2020. doi:10.1021/acs.nanolett.0c02472. URL <https://doi.org/10.1021/acs.nanolett.0c02472>. PMID: 32786939.
- [34] Yutaka Toyozawa. Theory of Line-Shapes of the Exciton Absorption Bands. *Progress of Theoretical Physics*, 20(1):53–81, 07 1958. ISSN 0033-068X. doi:10.1143/PTP.20.53. URL <https://doi.org/10.1143/PTP.20.53>.
- [35] Hsiao-Yi Chen, Davide Sangalli, and Marco Bernardi. Exciton-phonon interaction and relaxation times from first principles. *Phys. Rev. Lett.*, 125:107401, Aug 2020. doi:10.1103/PhysRevLett.125.107401. URL <https://link.aps.org/doi/10.1103/PhysRevLett.125.107401>.
- [36] Pierluigi Cudazzo. First-principles description of the exciton-phonon interaction: A cumulant approach. *Phys. Rev. B*, 102:045136, Jul 2020. doi:10.1103/PhysRevB.102.045136. URL <https://link.aps.org/doi/10.1103/PhysRevB.102.045136>.
- [37] Gabriel Antonius and Steven G. Louie. Theory of exciton-phonon coupling. *Phys. Rev. B*, 105:

- 085111, Feb 2022. doi:10.1103/PhysRevB.105.085111. URL <https://link.aps.org/doi/10.1103/PhysRevB.105.085111>.
- [38] Fulvio Paleari and Andrea Marini. Exciton-phonon interaction calls for a revision of the “exciton” concept. *Phys. Rev. B*, 106:125403, Sep 2022. doi:10.1103/PhysRevB.106.125403. URL <https://link.aps.org/doi/10.1103/PhysRevB.106.125403>.
- [39] Pierre Lechiffart, Fulvio Paleari, Davide Sangalli, and Claudio Attaccalite. First-principles study of luminescence in hexagonal boron nitride single layer: Exciton-phonon coupling and the role of substrate. *Phys. Rev. Mater.*, 7:024006, Feb 2023. doi:10.1103/PhysRevMaterials.7.024006. URL <https://link.aps.org/doi/10.1103/PhysRevMaterials.7.024006>.
- [40] Himani Mishra, Anindya Bose, Amit Dhar, and Sitangshu Bhattacharya. Exciton-phonon coupling and band-gap renormalization in monolayer wse₂. *Phys. Rev. B*, 98:045143, Jul 2018. doi:10.1103/PhysRevB.98.045143. URL <https://link.aps.org/doi/10.1103/PhysRevB.98.045143>.
- [41] Yang-hao Chan, Jonah B. Haber, Mit H. Naik, Jeffrey B. Neaton, Diana Y. Qiu, Felipe H. da Jornada, and Steven G. Louie. Exciton lifetime and optical line width profile via exciton-phonon interactions: Theory and first-principles calculations for monolayer mos₂. *Nano Letters*, 23(9):3971–3977, 2023. doi:10.1021/acs.nanolett.3c00732. URL <https://doi.org/10.1021/acs.nanolett.3c00732>. PMID: 37071728.
- [42] Hsiao-Yi Chen, Davide Sangalli, and Marco Bernardi. First-principles ultrafast exciton dynamics and time-domain spectroscopies: Dark-exciton mediated valley depolarization in monolayer wse₂. *Phys. Rev. Res.*, 4:043203, Dec 2022. doi:10.1103/PhysRevResearch.4.043203. URL <https://link.aps.org/doi/10.1103/PhysRevResearch.4.043203>.
- [43] Dominik Christiansen, Malte Selig, Gunnar Berghäuser, Robert Schmidt, Iris Niehues, Robert Schneider, Ashish Arora, Steffen Michaelis de Vasconcellos, Rudolf Bratschitsch, Ermin Malic, and Andreas Knorr. Phonon sidebands in monolayer transition metal dichalcogenides. *Phys. Rev. Lett.*, 119:187402, Nov 2017. doi:10.1103/PhysRevLett.119.187402. URL <https://link.aps.org/doi/10.1103/PhysRevLett.119.187402>.
- [44] Chiara Trovatello, Henrique P. C. Miranda, Alejandro Molina-Sánchez, Rocío Borrego-Varillas, Cristian Manzoni, Luca Moretti, Lucia Ganzer, Margherita Maiuri, Junjia Wang, Dumitru Dumcenco, Andras Kis, Ludger Wirtz, Andrea Marini, Giancarlo Soavi, An-

- drea C. Ferrari, Giulio Cerullo, Davide Sangalli, and Stefano Dal Conte. Strongly coupled coherent phonons in single-layer mos2. *ACS Nano*, 14(5):5700–5710, 05 2020. doi: 10.1021/acsnano.0c00309. URL <https://doi.org/10.1021/acsnano.0c00309>.
- [45] Donghai Li, Chiara Trovatello, Stefano Dal Conte, Matthias Nuß, Giancarlo Soavi, Gang Wang, Andrea C. Ferrari, Giulio Cerullo, and Tobias Brixner. Exciton–phonon coupling strength in single-layer mose2 at room temperature. *Nature Communications*, 12(1):954, 2021. doi:10.1038/s41467-021-20895-0. URL <https://doi.org/10.1038/s41467-021-20895-0>.
- [46] S. Mor, V. Gosetti, A. Molina-Sánchez, D. Sangalli, S. Achilli, V. F. Agekyan, P. Franceschini, C. Giannetti, L. Sangaletti, and S. Pagliara. Photoinduced modulation of the excitonic resonance via coupling with coherent phonons in a layered semiconductor. *Phys. Rev. Res.*, 3:043175, Dec 2021. doi:10.1103/PhysRevResearch.3.043175. URL <https://link.aps.org/doi/10.1103/PhysRevResearch.3.043175>.
- [47] Tae Young Jeong, Byung Moon Jin, Sonny H. Rhim, Lamjed Debbichi, Jaesung Park, Yu Dong Jang, Hyang Rok Lee, Dong-Hun Chae, Donghan Lee, Yong-Hoon Kim, Suyong Jung, and Ki Ju Yee. Coherent lattice vibrations in mono- and few-layer wse2. *ACS Nano*, 10(5): 5560–5566, 2016. doi:10.1021/acsnano.6b02253. URL <https://doi.org/10.1021/acsnano.6b02253>. PMID: 27102714.
- [48] Charles J. Sayers, Armando Genco, Chiara Trovatello, Stefano Dal Conte, Vladislav O. Khaustov, Jorge Cervantes-Villanueva, Davide Sangalli, Alejandro Molina-Sánchez, Camilla Coletti, Christoph Gadermaier, and Giulio Cerullo. Strong coupling of coherent phonons to excitons in semiconducting monolayer mote2. *Nano Letters*, 23(20):9235–9242, 2023. doi:10.1021/acs.nanolett.3c01936. URL <https://doi.org/10.1021/acs.nanolett.3c01936>. PMID: 37751559.
- [49] H. J. Zeiger, J. Vidal, T. K. Cheng, E. P. Ippen, G. Dresselhaus, and M. S. Dresselhaus. Theory for displacive excitation of coherent phonons. *Phys. Rev. B*, 45:768–778, Jan 1992. doi: 10.1103/PhysRevB.45.768. URL <https://link.aps.org/doi/10.1103/PhysRevB.45.768>.
- [50] A. V. Kuznetsov and C. J. Stanton. Theory of coherent phonon oscillations in semiconductors. *Phys. Rev. Lett.*, 73:3243–3246, Dec 1994. doi:10.1103/PhysRevLett.73.3243. URL <https://link.aps.org/doi/10.1103/PhysRevLett.73.3243>.
- [51] Kunie Ishioka and Oleg V Misochko. Coherent lattice oscillations in solids and their optical control: Part i. fundamentals and optical detection techniques. In *Progress in Ultrafast Intense*

- Laser Science: Volume V*, pages 23–46. Springer, 2009.
- [52] Gianluca Stefanucci, Robert van Leeuwen, and Enrico Perfetto. In and out-of-equilibrium ab initio theory of electrons and phonons. *Phys. Rev. X*, 13:031026, Sep 2023. doi: 10.1103/PhysRevX.13.031026. URL <https://link.aps.org/doi/10.1103/PhysRevX.13.031026>.
- [53] E. Perfetto, D. Sangalli, A. Marini, and G. Stefanucci. Pump-driven normal-to-excitonic insulator transition: Josephson oscillations and signatures of BEC-BCS crossover in time-resolved ARPES. *Phys. Rev. Materials*, 3:124601, Dec 2019. URL <https://link.aps.org/doi/10.1103/PhysRevMaterials.3.124601>.
- [54] G. Stefanucci and E. Perfetto. From carriers and virtual excitons to exciton populations: Insights into time-resolved ARPES spectra from an exactly solvable model. *Phys. Rev. B*, 103:245103, Jun 2021. doi:10.1103/PhysRevB.103.245103. URL <https://link.aps.org/doi/10.1103/PhysRevB.103.245103>.
- [55] Gianluca Stefanucci and Enrico Perfetto. Semiconductor electron-phonon equations: A rung above Boltzmann in the many-body ladder. *SciPost Phys.*, 16:073, 2024. doi: 10.21468/SciPostPhys.16.3.073. URL <https://scipost.org/10.21468/SciPostPhys.16.3.073>.
- [56] Andrea Marini. Equilibrium and out-of-equilibrium realistic phonon self-energy free from overscreening. *Phys. Rev. B*, 107:024305, Jan 2023. doi:10.1103/PhysRevB.107.024305. URL <https://link.aps.org/doi/10.1103/PhysRevB.107.024305>.
- [57] Tomasz Jakubczyk, Valentin Delmonte, Maciej Koperski, Karol Nogajewski, Clément Faugeras, Wolfgang Langbein, Marek Potemski, and Jacek Kasprzak. Radiatively limited dephasing and exciton dynamics in mose2 monolayers revealed with four-wave mixing microscopy. *Nano Letters*, 16(9):5333–5339, 2016. doi:10.1021/acs.nanolett.6b01060. URL <https://doi.org/10.1021/acs.nanolett.6b01060>. PMID: 27517124.
- [58] Tomasz Jakubczyk, Goutham Nayak, Lorenzo Scarpelli, Wei-Lai Liu, Sudipta Dubey, Nedjma Bendiab, Laëtitia Marty, Takashi Taniguchi, Kenji Watanabe, Francesco Masia, Gilles Nogues, Johann Coraux, Wolfgang Langbein, Julien Renard, Vincent Bouchiat, and Jacek Kasprzak. Coherence and density dynamics of excitons in a single-layer mos2 reaching the homogeneous limit. *ACS Nano*, 13(3):3500–3511, 2019. doi:10.1021/acsnano.8b09732. URL <https://doi.org/10.1021/acsnano.8b09732>. PMID: 30735350.

- [59] Enrico Perfetto and Gianluca Stefanucci. Real-time gw-ehrenfest-fan-migdal method for nonequilibrium 2d materials. *Nano Letters*, 23(15):7029–7036, 2023. doi: 10.1021/acs.nanolett.3c01772. URL <https://doi.org/10.1021/acs.nanolett.3c01772>. PMID: 37493350.
- [60] E. Perfetto, D. Sangalli, A. Marini, and G. Stefanucci. Nonequilibrium Bethe-Salpeter equation for transient photoabsorption spectroscopy. *Phys. Rev. B*, 92:205304, Nov 2015. doi: 10.1103/PhysRevB.92.205304. URL <https://link.aps.org/doi/10.1103/PhysRevB.92.205304>.
- [61] Alexey Chernikov, Arend M. van der Zande, Heather M. Hill, Albert F. Rigosi, Ajanth Velauthapillai, James Hone, and Tony F. Heinz. Electrical tuning of exciton binding energies in monolayer ws₂. *Phys. Rev. Lett.*, 115:126802, Sep 2015. URL <https://link.aps.org/doi/10.1103/PhysRevLett.115.126802>.
- [62] Eva A. A. Pogna, Margherita Marsili, Domenico De Fazio, Stefano Dal Conte, Cristian Manzoni, Davide Sangalli, Duhee Yoon, Antonio Lombardo, Andrea C. Ferrari, Andrea Marini, Giulio Cerullo, and Deborah Prezzi. Photo-induced bandgap renormalization governs the ultrafast response of single-layer mos2. *ACS Nano*, 10(1):1182–1188, 2016. doi: 10.1021/acsnano.5b06488. URL <https://doi.org/10.1021/acsnano.5b06488>.
- [63] Kaiyuan Yao, Aiming Yan, Salman Kahn, Aslihan Suslu, Yufeng Liang, Edward S. Barnard, Sefaattin Tongay, Alex Zettl, Nicholas J. Borys, and P. James Schuck. Optically discriminating carrier-induced quasiparticle band gap and exciton energy renormalization in monolayer mos₂. *Phys. Rev. Lett.*, 119:087401, Aug 2017. URL <https://link.aps.org/doi/10.1103/PhysRevLett.119.087401>.
- [64] A. Steinhoff, M. Rösner, F. Jahnke, T. O. Wehling, and C. Gies. Influence of excited carriers on the optical and electronic properties of mos2. *Nano Letters*, 14(7):3743–3748, 2014. URL <https://doi.org/10.1021/nl500595u>.
- [65] Valerie Smejkal, Florian Libisch, Alejandro Molina-Sanchez, Chiara Trovatello, Ludger Wirtz, and Andrea Marini. Time-dependent screening explains the ultrafast excitonic signal rise in 2d semiconductors. *ACS nano*, 15(1):1179–1185, 2020.
- [66] A. Steinhoff, M. Florian, M. Rösner, G. Schönhoff, T. O. Wehling, and F. Jahnke. Exciton fission in monolayer transition metal dichalcogenide semiconductors. *Nat. Commun.*, 8(1):1166, Oct 2017. URL <https://doi.org/10.1038/s41467-017-01298-6>.

- [67] Soungmin Bae, Kana Matsumoto, Hannes Raebiger, Ken-ichi Shudo, Yong-Hoon Kim, Ørjan Sele Handegard, Tadaaki Nagao, Masahiro Kitajima, Yuji Sakai, Xiang Zhang, Robert Vajtai, Pulickel Ajayan, Junichiro Kono, Jun Takeda, and Ikufumi Katayama. K-point longitudinal acoustic phonons are responsible for ultrafast intervalley scattering in monolayer mose2. *Nature Communications*, 13(1):4279, 2022. doi:10.1038/s41467-022-32008-6. URL <https://doi.org/10.1038/s41467-022-32008-6>.
- [68] Gui-Bin Liu, Wen-Yu Shan, Yugui Yao, Wang Yao, and Di Xiao. Three-band tight-binding model for monolayers of group-vib transition metal dichalcogenides. *Phys. Rev. B*, 88:085433, Aug 2013. doi:10.1103/PhysRevB.88.085433. URL <https://link.aps.org/doi/10.1103/PhysRevB.88.085433>.
- [69] Pierluigi Cudazzo, Ilya V. Tokatly, and Angel Rubio. Dielectric screening in two-dimensional insulators: Implications for excitonic and impurity states in graphane. *Phys. Rev. B*, 84: 085406, Aug 2011. doi:10.1103/PhysRevB.84.085406. URL <https://link.aps.org/doi/10.1103/PhysRevB.84.085406>.
- [70] S. Latini, T. Olsen, and K. S. Thygesen. Excitons in van der waals heterostructures: The important role of dielectric screening. *Phys. Rev. B*, 92:245123, Dec 2015. doi: 10.1103/PhysRevB.92.245123. URL <https://link.aps.org/doi/10.1103/PhysRevB.92.245123>.
- [71] Paolo Giannozzi, Stefano Baroni, Nicola Bonini, Matteo Calandra, Roberto Car, Carlo Cavazzoni, Davide Ceresoli, Guido L Chiarotti, Matteo Cococcioni, Ismaila Dabo, Andrea Dal Corso, Stefano de Gironcoli, Stefano Fabris, Guido Fratesi, Ralph Gebauer, Uwe Gerstmann, Christos Gougoussis, Anton Kokalj, Michele Lazzeri, Layla Martin-Samos, Nicola Marzari, Francesco Mauri, Riccardo Mazzarello, Stefano Paolini, Alfredo Pasquarello, Lorenzo Paulatto, Carlo Sbraccia, Sandro Scandolo, Gabriele Sclauzero, Ari P Seitsonen, Alexander Smogunov, Paolo Umari, and Renata M Wentzcovitch. Quantum espresso: a modular and open-source software project for quantum simulations of materials. *Journal of Physics: Condensed Matter*, 21(39): 395502, 2009. URL <http://stacks.iop.org/0953-8984/21/i=39/a=395502>.
- [72] E Perfetto and G Stefanucci. Cheers: a tool for correlated hole-electron evolution from real-time simulations. *J. Phys. Condens. Matter*, 30(46):465901, 2018. URL <http://stacks.iop.org/0953-8984/30/i=46/a=465901>.
- [73] E. Perfetto and G. Stefanucci. Some exact properties of the nonequilibrium response

- function for transient photoabsorption. *Phys. Rev. A*, 91:033416, Mar 2015. doi: 10.1103/PhysRevA.91.033416. URL <https://link.aps.org/doi/10.1103/PhysRevA.91.033416>.
- [74] C. Attaccalite, M. Grüning, and A. Marini. Real-time approach to the optical properties of solids and nanostructures: Time-dependent bethe-salpeter equation. *Phys. Rev. B*, 84: 245110, Dec 2011. doi:10.1103/PhysRevB.84.245110. URL <https://link.aps.org/doi/10.1103/PhysRevB.84.245110>.
- [75] Stefano Calati, Qiuyang Li, Xiaoyang Zhu, and Julia Stähler. Ultrafast evolution of the complex dielectric function of monolayer ws₂ after photoexcitation. *Phys. Chem. Chem. Phys.*, 23:22640–22646, 2021. doi:10.1039/D1CP03437E. URL <http://dx.doi.org/10.1039/D1CP03437E>.
- [76] L. V. Keldysh. Coulomb interaction in thin semiconductor and semimetal films. *Soviet Journal of Experimental and Theoretical Physics Letters*, 29:658, June 1979.
- [77] Timothy C. Berkelbach, Mark S. Hybertsen, and David R. Reichman. Theory of neutral and charged excitons in monolayer transition metal dichalcogenides. *Phys. Rev. B*, 88:045318, Jul 2013. doi:10.1103/PhysRevB.88.045318. URL <https://link.aps.org/doi/10.1103/PhysRevB.88.045318>.
- [78] Daniel Karlsson, Robert van Leeuwen, Yaroslav Pavlyukh, Enrico Perfetto, and Gianluca Stefanucci. Fast Green's function method for ultrafast electron-boson dynamics. *Phys. Rev. Lett.*, 127:036402, Jul 2021. doi:10.1103/PhysRevLett.127.036402. URL <https://link.aps.org/doi/10.1103/PhysRevLett.127.036402>.
- [79] E. Perfetto, Y. Pavlyukh, and G. Stefanucci. Real-time *gw*: Toward an ab initio description of the ultrafast carrier and exciton dynamics in two-dimensional materials. *Phys. Rev. Lett.*, 128:016801, Jan 2022. doi:10.1103/PhysRevLett.128.016801. URL <https://link.aps.org/doi/10.1103/PhysRevLett.128.016801>.
- [80] Y. Pavlyukh, E. Perfetto, Daniel Karlsson, Robert van Leeuwen, and G. Stefanucci. Time-linear scaling nonequilibrium green's function methods for real-time simulations of interacting electrons and bosons. i. formalism. *Phys. Rev. B*, 105:125134, Mar 2022. doi: 10.1103/PhysRevB.105.125134. URL <https://link.aps.org/doi/10.1103/PhysRevB.105.125134>.
- [81] Woojoo Lee, Yi Lin, Li-Syuan Lu, Wei-Chen Chueh, Mengke Liu, Xiaoqin Li, Wen-Hao Chang,

- Robert A. Kaindl, and Chih-Kang Shih. Time-resolved arpes determination of a quasi-particle band gap and hot electron dynamics in monolayer mos₂. *Nano Letters*, 21(17):7363–7370, 09 2021. doi:10.1021/acs.nanolett.1c02674. URL <https://doi.org/10.1021/acs.nanolett.1c02674>.
- [82] Fengcheng Wu, Fanyao Qu, and A. H. MacDonald. Exciton band structure of monolayer mos₂. *Phys. Rev. B*, 91:075310, Feb 2015. doi:10.1103/PhysRevB.91.075310. URL <https://link.aps.org/doi/10.1103/PhysRevB.91.075310>.
- [83] Falco Hüser, Thomas Olsen, and Kristian S. Thygesen. How dielectric screening in two-dimensional crystals affects the convergence of excited-state calculations: Monolayer mos₂. *Phys. Rev. B*, 88:245309, Dec 2013. doi:10.1103/PhysRevB.88.245309. URL <https://link.aps.org/doi/10.1103/PhysRevB.88.245309>.
- [84] Emilia Ridolfi, Caio H. Lewenkopf, and Vitor M. Pereira. Excitonic structure of the optical conductivity in mos₂ monolayers. *Phys. Rev. B*, 97:205409, May 2018. doi:10.1103/PhysRevB.97.205409. URL <https://link.aps.org/doi/10.1103/PhysRevB.97.205409>.
- [85] R. E. Groenewald, M. Rösner, G. Schönhoff, S. Haas, and T. O. Wehling. Valley plasmonics in transition metal dichalcogenides. *Phys. Rev. B*, 93:205145, May 2016. doi:10.1103/PhysRevB.93.205145. URL <https://link.aps.org/doi/10.1103/PhysRevB.93.205145>.
- [86] Jan M. Tomczak and Silke Biermann. Optical properties of correlated materials: Generalized peierls approach and its application to vo₂. *Phys. Rev. B*, 80:085117, Aug 2009. doi:10.1103/PhysRevB.80.085117. URL <https://link.aps.org/doi/10.1103/PhysRevB.80.085117>.
- [87] Xin-Bao Liu, Shi-Qi Hu, Daqiang Chen, Mengxue Guan, Qing Chen, and Sheng Meng. Calibrating out-of-equilibrium electron–phonon couplings in photoexcited mos₂. *Nano Letters*, 22(12):4800–4806, 2022. doi:10.1021/acs.nanolett.2c01105. URL <https://doi.org/10.1021/acs.nanolett.2c01105>. PMID: 35648107.